Information Systems and Engineering
Management Research Publications

Center of Excellence in Information Systems
and Engineering Management

6-1996

Flare energetics: analysis of a large flare on YZ Canis Minoris observed simultaneously in the ultraviolet, optical and radio.

G. H. J. van den Oord
Sterkundig Instuwt Utrecht

John G. Doyle
Armagh Observatory

M. Rodono
University of Catania

D. E. Gary
California Institute of Technology

Gregory W. Henry
Tennessee State University

See next page for additional authors

Recommended Citation

Authors

G. H. J. van den Oord, John G. Doyle, M. Rodono, D. E. Gary, Gregory W. Henry, Patrick B. Byrne, and Jeffrey L. Linsky

ASTRONOMY
AND
ASTROPHYSICS

Flare energetics: analysis of a large flare on YZ Canis Minoris observed simultaneously in the ultraviolet, optical and radio [*]

G.H.J. van den Oord[1], **J.G. Doyle**[2], **M. Rodonò**[3], **D.E. Gary**[4], **G.W. Henry**[5], **P.B. Byrne**[2], **J.L. Linsky**[6], **B.M. Haisch**[7], **I. Pagano**[3], and **G. Leto**[8]

[1] Sterrekundig Instituut Utrecht, Postbus 80.000, 3508 TA Utrecht, The Netherlands
[2] Armagh Observatory, College Hill, Armagh BT61 9DG, N. Ireland
[3] Istituto di Astronomia, Università di Catania, and Osservatorio Astrofisico di Catania, Viale A. Doria 6, I-95125 Catania, Italy
[4] California Institute of Technology, Solar Astronomy 264-33, Pasadena, CA 91125, USA
[5] Center of Excellence in Information Systems, Tennessee State University, Nashville, TN 37203, USA
[6] JILA, University of Colorado, and National Institute of Standards and Technology, Boulder CO-80309-0440, USA
[7] Lockheed Palo Alto Research Co., Palo Alto, CA 94304, USA
[8] Istituto di Radioastronomia C.N.R., Stazione VLBI, I-96017 Noto (SR), Italy

Abstract. The results of coordinated observations of the dMe star YZ CMi at optical, UV and radio wavelengths during 3 - 7 February 1983 are presented. YZ CMi showed repeated optical flaring with the largest flare having a magnitude of 3.8 in the U-band. This flare coincided with an IUE exposure which permits a comparison of the emission measure curves of YZ CMi in its flaring and quiescent state. During the flare a downward shift of the transition zone is observed while the radiative losses in the range $10^4 - 10^7$ K strongly increase. The optical flare is accompanied with a radio flare at 6 cm, while at 20 cm no emission is detected. The flare is interpreted in terms of optically thick synchrotron emission. We present a combined interpretation of the optical/radio flare and show that the flare can be interpreted within the context of solar two-ribbon/white-light flares. Special attention is paid to the bombardment of dMe atmospheres by particle beams. We show that the characteristic temperature of the heated atmosphere is almost independent of the beam flux and lies within the range of solar white-light flare temperatures. We also show that it is unlikely that stellar flares emit black-body spectra. The fraction of accelerated particles, as follows from our combined optical/radio interpretation is in good agreement with the fraction determined by two-ribbon flare reconnection models.

Key words: stars: YZ CMi; activity – atmospheres – late-type – flare – acceleration of particles

---

1. Introduction

Stars of different spectral type and luminosity class, e.g. B-type giants, RS CVn sub-giants, T Tauri stars and M dwarfs, have been observed to flare at all wavelengths. The basic characteristic shared by most of these flares is a rapid increase in emitted flux followed by a more gradual emission during the decay phase. In order to study the response of different atmospheric layers to the energy release during a flare, simultaneous observations covering as large a frequency range as possible are required. This calls for orchestrated campaigns during which the observing programs of various observatories are coordinated. Since flare activity is unpredictable such observing campaigns are not always successful. The multi–wavelength observations we analyse in this paper were obtained during a coordinated programme of simultaneous ultraviolet, optical and radio observations of late–type single and binary active stars, which successfully resulted in the detection of flares in all three wavelength bands on YZ CMi, AD Leo, V 1005 Ori (= Gliese 182) and AR Lac (Rodonò et al. 1984).

There have been several successful multi–wavelength campaigns for dMe stars involving YZ CMi (Kahler et al. 1982, Doyle et al. 1988), Prox Cen (Haisch et al. 1983), UV Ceti, AU Mic and BY Dra (Butler et al. 1986, 1987; De Jager et al. 1988), AD Leo (Rodonò et al. 1989) and EQ Peg (Haisch et al. 1987). Interesting physics can also be derived from single telescope observations, however, especially from optical (e.g. Houdebine et al. 1993a,b) or ultraviolet (Doyle et al. 1989, Linsky et al. 1989) spectroscopic data.

A widely accepted scenario for solar flares is that during the impulsive phase, beams of energetic electrons and/or protons are accelerated in the corona. When the fast electrons/protons are stopped in the high density chromosphere their energy is trans-
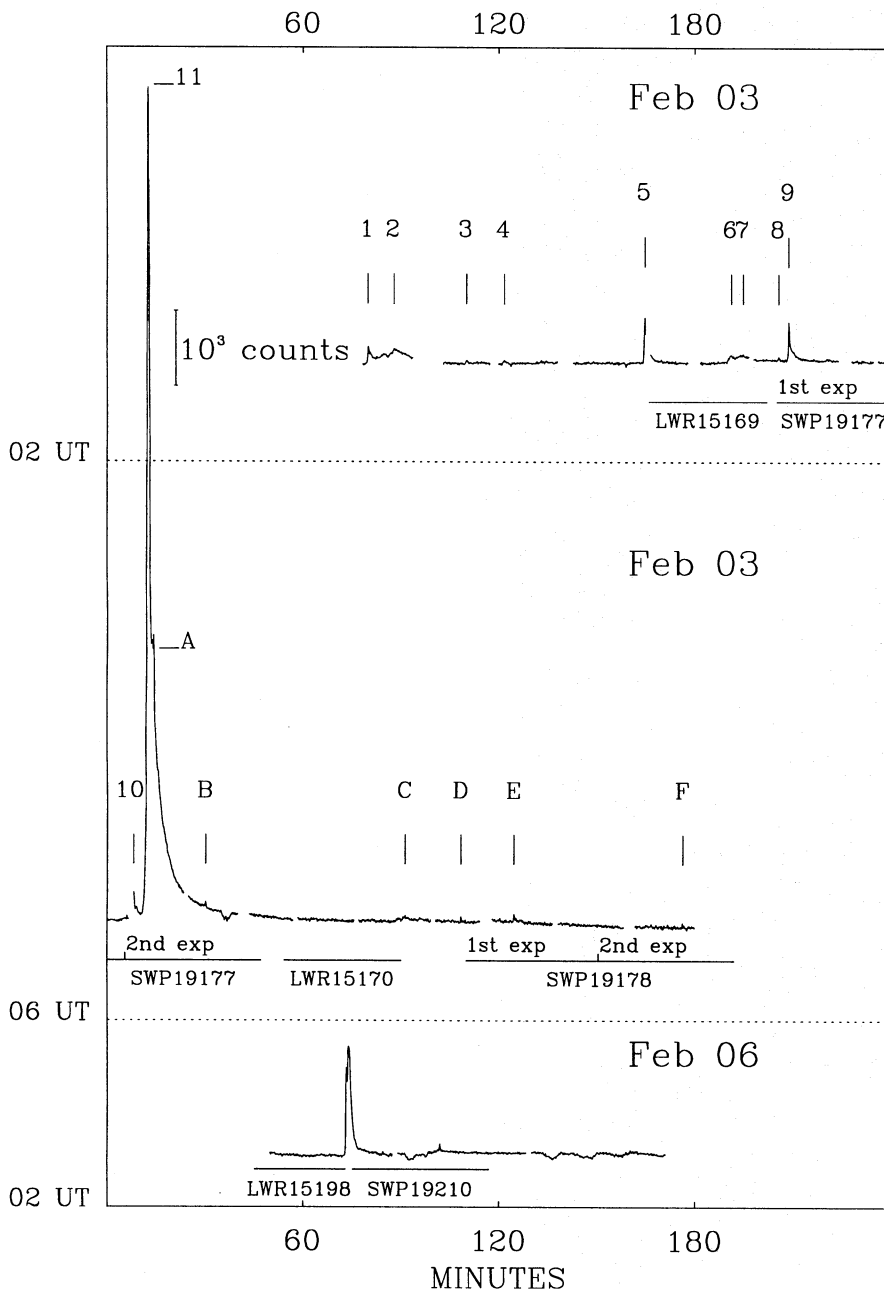
Fig. 1. The complete U-band light curve of YZ CMi on 3 and 6 February 1983, with *numbered vertical bars* identifying flare events. *Horizontal lines* indicate the time intervals of IUE exposures. *Capital letters* identify secondary peaks. On Feb. 3 frequent flaring activity is seen before the large flare (no. 11) occurred. The optical and simultaneous microwave light curves of this flare are shown on an enlarged scale in Fig. 2. Note that, after the rather faint and slow flare no. 6, YZ CMi remained about 10% brigther than pre-flare level. The large flare no. 11 was accompanied by a precursor event (no. 10) which had not completely decayed when the large flare occurred.

ferred to the ambient medium which is thereby heated. This interaction produces large pressure gradients which drive the heated material into the corona (commonly called evaporation) where it cools by radiation and conduction. The radiation from the 'evaporating' material then gives rise to the gradual phase of the flare with emission at soft X-ray, EUV and UV wavelengths. If the particle beams deposit their energy deep enough in the atmosphere a white-light flare may be observed. An alternative scenario for compact flares is one in which the energy release results in hot plasma confined between downward traveling conduction fronts. The fast electrons in the tail of the distribution cross the fronts and bombard the denser atmospheric layers, just as in the first scenario.

One should question whether these basic elements of solar flares can explain flares on dMe stars. This fundamental question was extensively addressed at IAU Colloquium No. 104 on *Solar and Stellar Flares* (Haisch and Rodonò 1989), where current models and interpretations of flare events are presented. For a discussion of the physical insight obtained from multi-wavelength flare observations we refer the reader to *Stellar Flares* (Pettersen 1991) and the Annual Review article by Haisch et al. (1991).

In this paper we present optical, UV and radio observations of YZ CMi in its quiescent and flaring state during 3 - 7 February 1983. We will concentrate on a large flare which we will compare with solar white-light flares. YZ CMi (Gl 285) is a dM4.5e star (Gliese 1969) with its Balmer lines in emission.
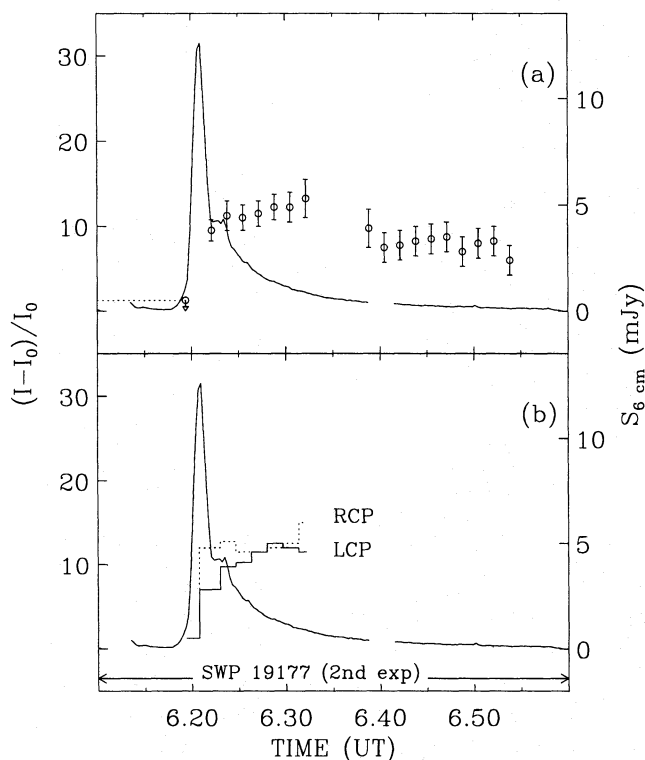
Fig. 2. a The U-band light curve of the 3 February 1983 YZ CMi flare (—), plus the VLA 6–cm data. **b** The RH & LH circular 6–cm polarization data.

Fig. 3. The double peaked YZ CMi flare observed on Feb. 6, 1983.

It is a member of both the UV Ceti class of flare stars and the group of BY Draconis-variables whose lightcurves show quasi-sinusoidal photometric variations.

The contents of this paper is as follows: in Sect. 2 we discuss the observations and the data reduction. In Sect. 3 the energetics are discussed in terms of the radiative losses in the optical and the UV, and for the observed radio-flare the source parameters are derived. A combined interpretation of the optical and the radio flare-data is presented in Sect. 4. Our conclusions are presented in Sect. 5.

2. Observational data and its reduction

2.1. Optical data

Several optical telescopes in Australia, Europe and U.S.A. were involved in the observation campaign during February 1983. The most successful flare monitoring was carried out at Mc-Donald Observatory in the Johnson U-band with the 0.9-m Cassegrain telescope. No flares were detected at the other observation sites. The McDonald observations were obtained with a 10–sec integration time on Feb. 3 (3:00 – 9:00 UT), Feb. 6 (2:50 – 5:07 UT), and Feb. 7 (3:00 – 6:00 UT). The typical accuracy of the McDonald U–band monitoring was $0^m.003$. YZ CMi was quite active on Feb. 3: ten relatively minor flares were observed before a large $\Delta U \sim 3.8$ flare occurred (see Fig. 1). This large flare (no. 11) occurred while a precursor event, possibly double-
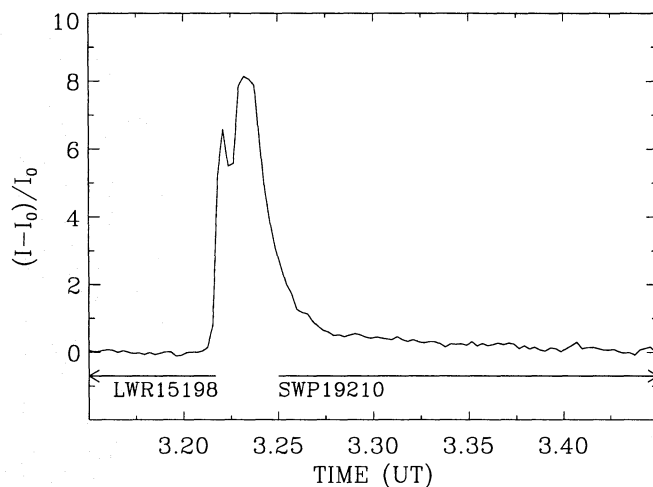
peaked, was still in its decay phase. The precursor flare appeared to peak at 06:08:10 UT, but the real maximum was very likely lost during sky measurements. The large flare started at about 06:10:45 UT, reached light maximum at 06:12:35 UT, and then decayed to pre–flare level in about 35 min.

After the relatively small precursor flare, the star remained about 20% brighter than the pre–flare level. We note, however, that this pre–flare level was already about 10% brighter than the supposedly quiescent level at the beginning of the observation run. In fact, after flare no. 6, which was quite faint and slow, without any spiky fast phase, YZ CMi did not return to its quiescent level, while other minor flares (nos. 7 to 9) and the large flare occurred.

On February 6, YZ CMi was much less active, since only a moderately intense flare ($\Delta U \sim 2.2$) with double–peaked light profile was observed (see Fig. 3). On February 7, no flares at all were detected. The principal characteristics of the observed flares are given in Table 1. The flare energies were derived by time integrating their U–band light curves and assuming U=13.8 for the quiescent U–band magnitude and a distance of 6.2 pc (Gliese 1969). These parameters imply a quiescent U–band luminosity of 3.23×10^{28} erg s^{-1} according to the flux calibration of Bessell (1979).

2.2. Radio data

Microwave monitoring was carried out with the VLA in its C configuration. The 27 antennas of the VLA were divided into two subarrays, one operating at 6 cm (4.89 GHz), and the other operating at 20 cm (1.47 GHz). Two of the antennas were not working, leaving 12 antennas in the 6 cm subarray, and 13 antennas in the 20 cm subarray. The data were calibrated in absolute flux by reference to 3C 286, and the phase calibrator was 0742+103. Phase calibrator observations occurred every 30 min. The source signal at 6 cm before the large optical flare (no. 11) was consistent with YZ CMi's known *quiescent* upper limit of a few tenths of a mJy at 6 cm. The 6 cm light curve during the optical flare is shown in Fig. 2a, and the RH and LH

Table 1. Characteristics of the YZ CMi flares observed at McDonald Observatory in the period 3-7 February 1983.

Date 1983	no.	$(U.T.)_{max}$ (h:m:s)	$\left(\frac{I_f - I_o}{I_o}\right)_{max}$	ΔU	t_{rise} (min)	t_{decay} (min)	P (Eq. 1) (min)	Comments
Feb. 3	1	3:19:45	0.77	0.62	0.3	3.	–	1st peak
	2	3:27:45	0.26	0.25	1.3	15.	5.92	sec. peak
	3	3:50:05	0.15	0.15	0.5	1.	0.12	faint flare
	4	4:01:45	0.22	0.21	0.7	2.	0.26	faint flare
	5	4:44:45	1.88	1.15	1.3	9.	1.43	faint flare
	6	5:11:05	0.28	0.27	1.3	>30	(^{b})	1st peak, long-duration decay
	7	5:14:45	0.25	0.24	1.3	(^{a})	1.05	secondary peak
	8	5:25:25	0.14	0.14	0.4	(^{a})	0.09	secondary peak
	9	5:28:35	1.46	0.98	0.3	(^{a})	1.62	
	10	6:08:05	1.05	(0.78)	—	2.	(^{b})	precursor flare, max lost
	11	6:12:35	31.76	3.79	1.8	35.	78.92	multi-peaked, largest flare
Feb. 6	1	3:13:55	8.59	2.20	1.4	12.	16.7	double-peaked

(^{a}) secondary peak during flare no. 6 decay phase
(^{b}) P value included in the subsequent secondary peak

circular polarization data are presented in Fig. 2b. Observations of the decay of the radio flare were interrupted by a calibration observation, which took place from 06:20-06:23 UT, some 8-9 minutes after the peak of the U-band burst. The burst was still in progress at 6 cm after returning from the calibrator at 06:23 UT. Although the observations were taken with 3 sec time resolution, the burst was sufficiently weak that its flux at 6 cm was measurable only on maps with 1 min or longer integration time. The 1σ noise level of these 1-min maps, after cleaning, was 0.5-0.7 mJy in each sense of circular polarization. The burst was not detected at 20 cm. At 6 cm, the flare reached its peak intensity about 7 mins. later than the U-band peak. Polarization measurements show a slight RH circular polarization excess during most of the flare, except just before its peak emission. Given the noise level, this excess RH polarization is not statistically significant.

2.3. Ultraviolet spectroscopy

Table 2 provides a list of SWP and LWR low-dispersion UV spectra of YZ CMi obtained with the International Ultraviolet Explorer satellite in February 1983. Here we concentrate mostly on the two separate spectra obtained sequentially on image SWP19177: the first spectrum appears rather quiescent, while the large flare and its precursor strongly affect the second 40–min exposure. The two exposure time–intervals are shown as horizontal bars in Fig. 1. During the first 40–min exposure no strong flare activity was observed in the U-band, where the second 40-min exposure included the entire duration of flares no. 10 and no. 11. All of the remaining images listed in Table 2 show no signs of flare activity, most likely because the exposure times were purposely kept short to avoid saturation due to large flares. The spectra of the usable images listed in Table 2 were extracted from the photometrically corrected IUE images using the IUEDR computer program on the UK STARLINK computer network (Giddings 1989). Since the nominal resolution of the

IUE spectrograph in low resolution mode is $\sim$ 4.2Å, the final extracted spectra were slightly smoothed, using a Gaussian with a FWHM of 3.5Å, in order to reduce the noise.

The extracted spectra were further analyzed using the STARLINK DIPSO program (Howarth & Murray 1990). Line fluxes for the prominent SWP emission lines were derived by least squares Gaussian fits. This procedure gives similar results to a summation under the line for strong unblended lines, although gaussian fits are considered to be superior. The fitting procedure was carried out by estimating the width and center of the line, which were subsequently optimized to produce the best fit. An estimated continuum contribution was removed from the data before the line parameters were measured. The derived line fluxes at Earth were converted to surface fluxes at the star using the conversion factor, $F/f = 5.75\ 10^{17}$ from Mathioudakis & Doyle (1992). The flare spectrum and the mean quiescent spectrum are shown in Fig. 4, where the *quiescent* spectrum is the mean of the three nonflare SWP spectra taken on February 3. The individual line fluxes for the quiescent and flaring states are presented in Table 3.

3. Results

In this section we derive various parameters for the large flare (no. 11) on 3 February 1983.

3.1. Optical flare energy

The flare's equivalent duration P is given by (Gershberg 1972)

$$P = \sum_f [(I_f - I_o)/I_o]\Delta t \qquad (1)$$

where I_o is the observed countrate from the star in its quiescent state after sky subtraction, I_f the countrate due to the star in its flare state less sky background, and Δt is the U-band
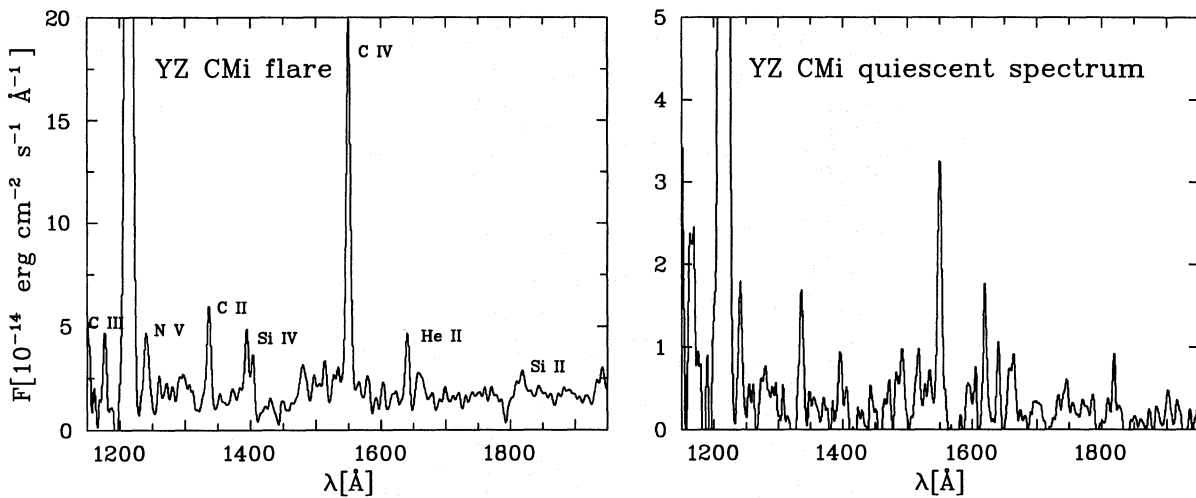
Fig. 4. a The IUE SWP flare spectrum for the YZ CMi event of 3 February 1983 starting at 06:06 UT and **b** the mean quiescent spectrum.
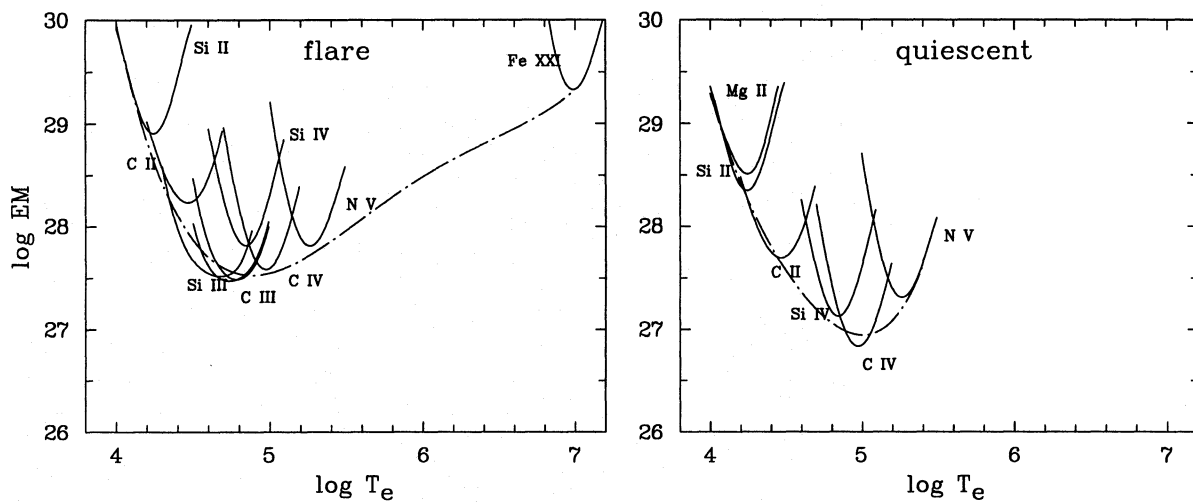

Fig. 5. a The YZ CMi flare EM curve (note that the flare EM must be multiplied by $1/f = 4\pi R_*^2/A_{\text{flare}}$ where f is the flare filling factor in the UV); **b** the EM curve for YZ CMi in quiescence. The flare EM curve above $3\ 10^5$ K is very uncertain since it is only based on the upper limit of the Fe XXI line at 1354Å.

integration time. Taking the quiescent U-band luminosity of $3.23\ 10^{28}$ erg s^{-1}, as derived in Sect. 2.1, the flare's equivalent duration (P = 4735 sec) implies a flare energy of $1.5\ 10^{32}$ erg in the U-band. This is a lower limit to the total emitted optical energy. Although flares are unique events that sometimes show unusual time and colour behaviour, statistical studies based on large collections of flare data (e.g. Lacy et al. 1976) indicate that the mean ratio between the total energy emitted in the optical UBV–bands and the energy emitted in the U–band is $E_{\text{opt}}/E_{\text{U}} = 2.4$. Thus for the YZ CMi flare we derive $E_{\text{opt}} = 3.6\ 10^{32}$ erg.

3.2. Radio flare

It is interesting that during the optical flare a radio burst was detected at 6 cm while no indications were found for radio

emission at 20 cm. The apparent weak excess of RH circular polarization during the burst is not a statistically significant 3σ-detection. The gradual time profile of the burst, in combination with the absence of strong circular polarization and the moderate flux at the maximum of the burst, makes it unlikely that the observed emission is coherent but one-minute integrations are not ideal to detect spikes of coherent emission, if present, since the time profile of a burst depends strongly on the integration time. An example of this is the observation by van den Oord and de Bruyn (1994) who detected coherent emission at 360 MHz from II Peg. In one-minute integrations a highly variable flux was observed, while with four-minute integrations the burst showed a very smooth time profile (see their Figs. 2 and 4). That example demonstrates that the spikey nature of coherent emission can be completely masked when integration times longer than the characteristic time scale of the emission are used.

Table 2. Log of IUE SWP & LWP low-dispersion spectra of YZ CMi on multiple–exposure images obtained in February 1983. The start time (U.T.) of the first exposure on each multiple–exposure image is listed.

Date	Image No.	U.T.	t_{exp}[+] (min)	Comments
Feb. 3	LWR15169	04:46	4× 8	
	SWP19177	05:25	2×40	large flare on 2nd exp.
	LWR15170	06:54	4× 8	
	SWP19178	07:50	2×40	weak spectra
Feb. 6	LWR15198	02:45	4× 6	
	SWP19210	03:15	2×20	too weak spectra
Feb. 7	LWR15205	03:50	8	weak spectrum
	LWR15206	04:34	2× 8	
	LWR15207	05:25	4× 5	

[+] t_{exp} = no. of exposures × each segment exp. time

Therefore we looked for variability using 10 sec. maps but no indications for spike emission were found. The fluxes quoted in this paper are based on one minute maps which provide a reasonable compromise between S/N and time resolution.

For the present observation the brightness temperature at 6 cm is

$$T_b = \frac{c^2}{2k\nu^2} \frac{d^2}{\chi_r \pi R_*^2} F = 2.4 \ 10^8 \frac{F_{mJy}}{\chi_r} \ \text{K} \quad (2)$$

with $d = 6.2$ pc the distance of the star, $R_* = 0.37 R_\odot$ the radius of the star, F the observed flux (F_{mJy} when expressed in mJy) and χ_r the source area of the radio emission normalized on the stellar disk area. At the maximum of the flare the brightness temperature was approximately 10^9 K if the source were the size of the stellar surface. For a smaller radio source the brightness temperature would even be higher. These values of the brightness temperature indicate that the emission is neither thermal nor coherent. A more likely interpretation is that the observed emission is synchrotron radiation from a non-thermal particle population as is often thought to be responsible for radio flares. In the case of optically thick synchrotron emission by a mono-energetic particle population the observed flux is (Pacholczyk, 1970)

$$F = \frac{\chi_r \pi R_*^2}{d^2} \frac{\nu^{5/2}}{c^2 \sqrt{c_1 B \sin \vartheta}} x^{-5/2} S(x) \ , \quad (3)$$

where B is the magnetic field strength, ϑ the angle between the field and the ray, $c_1 = 6.27 \ 10^{18}$ a constant, $S(x) = x \int_x^\infty K_{5/3}(z)dz/K_{5/3}(x)$ with $K_{5/3}$ a Bessel function of the second kind, and $x = \nu/\nu_{crit}$. $\nu_{crit} = c_1 B \sin \vartheta E^2$ is the critical frequency which appears in the expression for synchrotron emission. The particle energy is indicated by E. The observed flux of ~ 5 mJy at 6 cm indicates that the particle energy is $E = 0.9/\sqrt{B_2 \sin \vartheta}$ MeV when $\chi_r = 1$ ($x = 4$) and $E = 2.4/\sqrt{B_2 \sin \vartheta}$ MeV when $\chi_r = 0.1$ ($x = 0.52$). Here $B_2 = B/100$. The derived particle energies are only weak functions of the assumed field strength and the flare area. We con-

Table 3. UV line fluxes for YZ CMi (10^{-13} erg cm^{-2}s^{-1}) on 3 February 1983. The quiescent fluxes are derived from the first exposure of SWP19177 and the two exposures of SWP19178. For the flare the fluxes are derived from the second exposure of SWP19177.

Ion (Å)	Quiescent	Flare
C III 1176[+]	–	3.21
Si III 1205	–	<2.54
N V 1240[*]	1.18	3.72
C II 1335[+]	1.32	4.55
C I/Fe XXI 1354	–	<0.76
Si IV 1393	<0.67	4.55
Si IV 1402	<0.34	3.27
C I 1513	–	2.35
Si II 1526	–	<1.48
Si II 1533	–	<1.71
C IV 1550[*]	2.83	15.80
C I 1561	–	0.59
He II 1640	0.67	3.34
C I 1656	–	1.32
Si II 1809	0.23	1.12
Si II 1818	0.55	1.74
C III 1907	–	<0.28
Fe II 1915	–	0.24
C I 1933	–	0.84
Cont. 1160–1960Å	....	59.2

(from LWR spectra)

Fe II 2600[+*o]	5.40	–
Mg II 2800 [*o]	9.30	–

[*]doublet
[+]multiplet
[o]mean from six spectra with 2.0 rms

clude that the 6 cm flux is compatible with synchrotron emission from particles with energies of a few MeV.

Our assumption that the flux at 6 cm is optically thick needs to be checked by considering the absorption coefficient for synchrotron radiation (Pacholczyk, 1970),

$$\kappa = 4.2 \ 10^7 (B \sin \vartheta)^{3/2} \nu^{-5/2} n_f x^{5/2} K_{5/3}(x) \ \text{cm}^{-1}$$
$$= 2.5 \ 10^{-14} (B_2 \sin \vartheta)^{3/2} n_f x^{5/2} K_{5/3}(x) \ \text{cm}^{-1} \ , \quad (4)$$

where the last identity applies to 6 cm observations. In this expression n_f is the density of the fast particles emitting the synchrotron radiation. By writing the optical depth at 6 cm as $\tau_6 = \kappa \ell R_*$ with ℓ the source size along the line of sight (expressed in stellar radii), we find that $\tau_6 > 1$ when $n_f \ell \gtrsim 2 \ 10^3$ cm^{-2}. This is a rather small number indicating that it is likely that the source is indeed optically thick.

3.3. Emission Measure Analysis

Emission measure (EM) curves were constructed using the tabulation of flux versus pressure for a constant EM from Doyle

& Keenan (1992) and the corresponding contribution functions, i.e.

$$EM = \frac{F_{obs}(\lambda)}{F_{pred}(\lambda)} \, 10^{26} \text{ cm}^{-5} , \qquad (5)$$

where $F_{obs}(\lambda)$ is the observed flux at wavelength λ and $F_{pred}(\lambda)$ is the value given in the tables of Doyle & Keenan. The emission measure curve for an electron pressure of 10^{15} cm^{-3}K is shown in Fig. 5 for both the flare and (mean) quiescent periods. Note that in the flare, the only electron density sensitive line is the very weak (hence only an upper limit to the flux can be given) C III 1908Å line. The electron pressure was therefore based on the C III 1176/C III 1908 ratio. On the other hand if we were to use the Si IV 1394/C III 1908 ratio, an electron pressure of a factor of 3 higher than the above would be implied. Density sensitive lines are not seen in our faint quiescent spectra.

At the formation temperature of C III, this pressure implies an electron density of $\sim 2 \, 10^{10}$ cm^{-3}. This is rather low compared to the derived electron density of some RS CVn flares (e.g. see Doyle et al. 1989, Linsky et al. 1989), but since the IUE spectrum was of 40–min duration and the flare was entirely contained within this time interval, it is possible that much higher densities were present during the rise phase, as is found in solar flares (Wolfson et al. 1983). The EM curve for temperatures above $3 \, 10^5$ K is very uncertain because the only data point available is the upper limit to the Fe XXI line at 1354Å which could also have a large contribution from C I (cf. the GHRS spectrum of AU Mic obtained by Maran et al. 1994). It is important to note that, when deriving the emission measure curves, solar abundances are usually assumed, but Meyer (1985) has shown that there is a depletion in the solar coronal abundances of certain elements relative to the photosphere. In our emission measure curves such abundance variations would mainly affect the curves of ions of C and N for which Meyer finds that the ratio of photospheric to coronal abundances is a factor of 2 or greater. The present data set does not permit us to check for abundance variations, but in general the shape of the EM curve is represented satisfactorily by the assumption of coronal abundances (Cook et al. 1989) and it is from this data that the subsequent analysis is carried out. We note that Linsky et al. (1995) found that coronal abundances lead to a better fit to the emission measure distribution for the Capella G1 III component.

3.4. Radiative losses

The radiative losses in the part of the atmosphere 'covered' by the EM curve may be estimated by multiplying the EM by the radiative loss function. The radiative loss function used here is that due to Cook et al. (1989). The derived values for YZ CMi in different parts of the atmosphere are given in Table 4. In order to derive the total radiative losses, the values in Table 4 should be multiplied by the surface area of the star. This gives for the quiescent state radiative losses of at least $1.3 \, 10^{29}$ erg s^{-1} and for the flare $2.9 \, 10^{29}$ erg s^{-1} over the temperature range $4.0 \leq \log T_e \leq 5.4$. Over the temperature range $5.5 \leq$
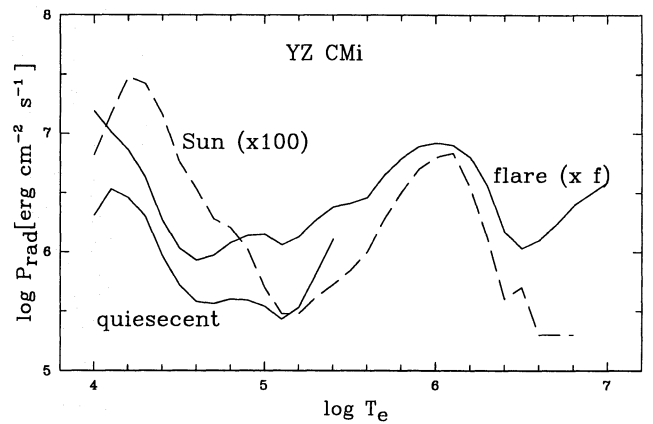

Fig. 6. The surface radiative losses for the flare and the quiescent state of YZ CMi based on the IUE fluxes. For the calculation of the flare radiative losses the flare area is taken equal to the surface area of the star. The flare filling factor is given by $f = A_{flare}/(4\pi R_*^2)$.

$\log T_e \leq 7.0$, we have additional flare radiative losses of $\sim 5.1 \, 10^{29}$ erg s^{-1}. Note that the quiescent value has not being subtracted from this latter figure. Also none of these figures include losses due to Ca II H&K, and especially for a dMe star, the Hydrogen Lyman and Balmer lines. During the flare, the continuum losses over the wavelength range $1160 - 1960$Å (see Table 3) amount to $\sim 2.7 \, 10^{28}$ erg s^{-1}. The U-band data implies losses of $3.6 \, 10^{32}$ erg in the optical UBV bands, giving total radiative losses over the flare event of at least $2.3 \, 10^{33}$ erg.

In Fig. 6 we plot the surface radiative losses function of temperature as derived from the IUE data. Again we note that at $\log T_e > 5.5$ the radiative losses presented in Fig. 6 and Table 4 are subject to considerable uncertainties due to lack of line diagnostics. During the flare the total radiative losses add up to $1.2 \, 10^8$ erg cm^{-2}s^{-1} in the temperature range $4 \leq \log T_e \leq 7$ (see Table 4). Bruner and McWhirther (1988) derived an empirical relation between the C IV line flux and the total radiative losses in the range $4 \leq \log T_e \leq 8$ with an accuracy of a factor two. Using the observed C IV line flux gives for YZ CMi in its quiescent state a total radiative loss of $4.1 \, 10^7$ erg cm^{-2}s^{-1} at temperatures above 10^4 K. For the flare + quiescent the radiative losses amount to $2.6 \, 10^8$ erg cm^{-2}s^{-1} which is, despite the uncertainties, only a factor 2.2 larger than the value which follows from Table 4.

4. Interpretation

It is interesting to see whether the present data permit the construction of a simple model for the observed flare. For solar flares the white light emission is caused by the bombardment of the chromosphere/photosphere by beams of energetic particles. A second energetic particle population causes the non-thermal radio emission in the corona. Both energetic particle populations are thought to be energized during the reconnection process by direct electric field (run-away) acceleration in a current sheet. This statement does not relate to the coherent emission by e.g.

Table 4. Surface radiative losses for YZ CMi during the flare and in quiescence. Comparison figures are also given for the Sun as derived by Quin et al. (1993). Note that the surface area assumed for the flare is that of the whole stellar surface. The radiative losses at $\log T_e > 5.5$ are very uncertain and should be considered as a rough estimate (see Sect. 3.4 for an estimate of the total flare radiative losses).

Atmospheric region	Temperature range	Radiative losses (10^6 erg cm^{-2}s^{-1})		
		YZ CMi (flare + quiescent)	YZ CMi (quiescent)	Sun
upper chromosphere	$4.0 \leq \log T_e \leq 4.5$	40.2	11.8	2.2
mid T-R	$4.6 \leq \log T_e \leq 5.4$	12.5	4.4	0.3
upper T-R/lower corona	$5.5 \leq \log T_e \leq 6.0$	(32.2)	....	0.2
upper corona	$6.0 \leq \log T_e \leq 7.0$	(32.1)	....	0.1

shock acceleration. The largest solar flares, that is, those which show white light emission, are related to a filament eruption and are called two-ribbon flares. The scenario for a two-ribbon flare is conceptually simple and may be well suited for an application to stellar flares: as a filament evolves it can reach a critical height after which it becomes unstable (van Tend and Kuperus, 1978). The point of instability is characterized by the occurrence above the photosphere of a neutral line, which is unstable and quickly collapses into a neutral sheet (Syrovatskii, 1981). As the filament moves upward, magnetic field lines from the topologically different regions on both sides of the sheet move towards the current sheet and reconnect. This 'cutting' of field lines due to reconnection permits the filament to move upward, since the reconnected field lines are not connected to the photosphere. Below the current sheet a growing arcade of loops is formed while above the current sheet a plasmoid surrounding the filament moves upward. In this scenario the filament is located at an O-type neutral point and the current sheet at a collapsed X-type neutral point. This model was first worked out by Kaastra (1985) and later extended by Martens (1986), Martens and Kuin (1989), Forbes (1990, 1991) and Forbes and Isenberg (1991).

Since our limited data set does not permit a detailed comparison with solar two-ribbon flares we use the basic concepts of the two-ribbon flare to link the observed optical and radio emission. For that purpose we assume that the acceleration process in the current sheet results in a particle population with a typical energy E. When these particles leave the reconnection site they emit the observed synchrotron radiation in the ambient magnetic field. Those particles with sufficiently small pitch-angles can enter the loss cones of the newly formed loops below the current sheet and precipitate into the chromosphere/photosphere where they lose their energy by Coulomb collisions and heat the plasma. This heated plasma lies at the origin of the optical flare emission. We now make the assumption that the optical emission has a black-body spectrum. The validity of this assumption is discussed later in this paper.

In Sect. 3.2 we found that, depending on the assumed size of the radio source, the typical particle energy is about one to a few MeV. Table 5 lists the exact numbers for the cases that $\chi_r = 0.1$ and $\chi_r = 1$, but for the range considered the particle

energy does not depend strongly on the assumed source size. Let us assume, therefore, that the acceleration process results in particles with an energy of about one MeV. The particles which remain in the coronal volume and do not precipitate to denser layers are responsible for the radio flare. These particles will predominantly lose their energy by collisions in the corona which for 0.1 - 10 MeV electrons occurs on a characteristic timescale given by (Benz and Gold, 1971)

$$t_{col} = 1.59 \; 10^{12} E n^{-1} \qquad (6)$$

with E the particle energy in MeV and n the ambient coronal density. A linear regression fit for an assumed exponential decay of the 6 cm flux gives a characteristic decay time of 1322 seconds. Equating this decay time to the collisional time scale results in a coronal density of $n \approx 10^9$ cm^{-3}, which corresponds to a plasma frequency of $\nu_p \approx 0.3$ GHz. The absence of flare emission at 1.47 GHz is therefore not due to the observing frequency being below the local plasma frequency. The synchrotron emission at a given frequency can be strongly depressed because of the reduced phase velocity in a plasma, the so-called Razin supresion at frequencies $\nu \lesssim 20n/B \approx 0.2n_9/B_2$ GHz. This frequency is also below the observing frequencies, so that the absence of detected 20 cm emission can not be attributed to the Razin effect.

If our assumption that the source is optically thick at 6 cm is true, then the source must also be optically thick at 20 cm. Using Eq. (3) we find that at the maximum of the radio flare, when the 6 cm flux amounts to ~ 5 mJy, the 20 cm flux equals $F_{20} = 1/\sqrt{B_2 \sin \vartheta}$ mJy for $\chi_r = 1$ or $F_{20} = 0.6/\sqrt{B_2 \sin \vartheta}$ mJy for $\chi_r = 0.1$. Given the noise levels in the one-minute maps ($\sim 0.5 - 0.6$ mJy), these fluxes will not result in a statistically significant detection. It is important to note that the absence of emission at 20 cm is compatible with an interpretation in terms of optically thick synchrotron emission and does not require a (narrow bandwidth) coherent mechanism.

Next we turn to the optical emission. Those particles which precipitate into the loss cone loose their energy over a column depth (Emslie,1978; van den Oord, 1988)

$$N = \frac{E^2 \mu_0}{6\pi e^4 \Lambda} = 1.28 \; 10^{23} \left(\frac{\Lambda}{20}\right)^{-1} \left(\frac{E}{1 \text{ MeV}}\right)^2 \quad \text{cm}^{-2} \; , \quad (7)$$

where μ_0 is the cosine of the pitch-angle at the moment of injection (here taken unity), E is the energy at the moment of injection, e is the electron charge, and Λ is the Coulomb logarithm. This expression shows that MeV particles can traverse substantial column densities and, as a consequence, deposit energy at a substantial depth in the atmosphere. The atmospheric volume where the beam energy is deposited will heat up, but in the atmosphere of a dMe star a considerable fraction of the beam energy will go into the ionization of the (abundant) neutral hydrogen. The most energetic beam particles are stopped in the deepest layers where a strong temperature gradient is created since the beam energy input, and therefore the heating, stops there. This temperature gradient drives a conductive energy flux out of the heated plasma column. A simple model for the temperature evolution of the (beam) heated plasma column was proposed by van den Oord (1988) who considered the energy balance of the heated volume

$$\frac{3}{2} N k \frac{dT}{dt} = F_{\text{b}} - F_{\text{sat}} - F_{\text{ion}} \quad \text{erg cm}^{-2} \text{ s}^{-1} \; , \quad (8)$$

where F_{b} is the beam energy flux, $F_{\text{sat}} = \left(\frac{2}{\pi}\right)^{1/2} n_{\text{e}} m_{\text{e}} \left(\frac{kT}{m_{\text{e}}}\right)$ is the saturated heat flux and F_{ion} is the ionization loss. The temperature gradient at the bottom of the heated volume is so large that classical heat conduction theory breaks down and the classical conduction should be replaced by the saturated heat flux (for a discussion see van den Oord, 1988). The ionization equilibrium is determined by an (instantaneous) balance between collisional ionization and radiative recombination. Direct ionization of hydrogen by the beam particles is neglected in this model but for the energy balance it is not important whether the beam energy goes directly into ionization energy or first into heat and then into ionization energy. The system quickly evolves towards an equilibrium temperature set by the balance of beam heating and conductive and ionization losses: $F_{\text{b}} - F_{\text{sat}} - F_{\text{ion}} = 0$. This equilibrium temperature is completely determined by the beam parameters: the beam flux F_{b}, and the energy of the beam particles E. This energy determines the column depth over which the beam heating takes place (cf. Eq. (7)). The equilibrium equation reads (see van den Oord, 1988)

$$F_{\text{b}} - \left(\frac{2}{\pi}\right)^{1/2} m_{\text{e}} \left(\frac{k}{m_{\text{e}}}\right)^{3/2} N_{\text{H}} \left(\frac{f}{f+1}\right) T^{3/2}$$
$$- \alpha N_{\text{H}} N \chi \left(\frac{f}{f+1}\right)^2 = 0 \; , \quad (9)$$

where N is the column density (cm^{-2}), N_{H} is the total (neutral and ionized) hydrogen density (cm^{-3}), χ is the ionization potential of hydrogen (13.6 eV), and $f = C/\alpha$ with
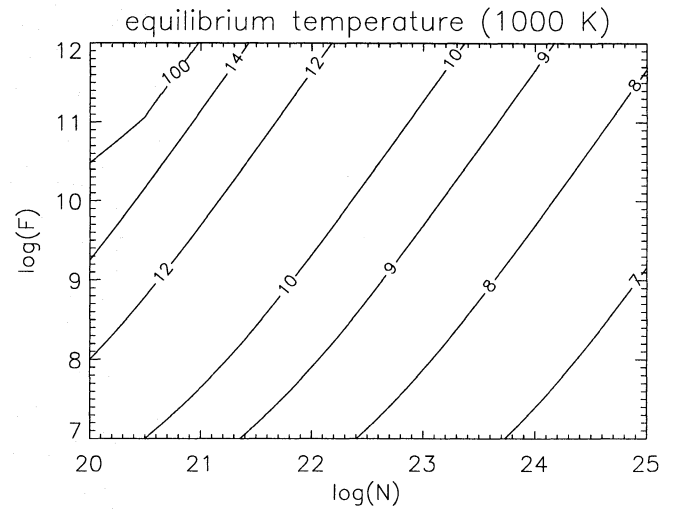

Fig. 7. Equilibrium temperature reached by a plasma column subjected to beam injection as a function of the beam flux F and the column density N. The labels for the contour levels are in units of 1000 K.

$C = 10^{-10} T^{1/2} e^{-y}$ the collisonal ionization coefficient and $\alpha = 2 \; 10^{-11} T^{-1/2} \varphi(y)$ the radiative recombination coefficient, $y = \chi/kT$ and $\varphi(y)$ is a slowly varying function of the temperature. The expressions for α and C are taken from Tucker (1975). The total hydrogen density N_{H} can be related to the column density using $N_{\text{H}} \approx 2 \; 10^{-7} N$ which follows from a fit to a model atmosphere for YZ CMi by Giampapa et al. (1982). (This relation differs by a factor two with the relation used by van den Oord, 1988). The above expression can now be written as

$$F_{\text{b},11} - 8.5 \; 10^{-8} N_{21} \left(\frac{f}{f+1}\right) T^{3/2}$$
$$- 868 N_{21}^2 \left(\frac{f}{f+1}\right)^2 T^{-1/2} = 0 \; , \quad (10)$$

where $F_{\text{b},11} = F_{\text{b}}/10^{11}$ and $N_{21} = N/10^{21}$. For a given beam flux and column density (or beam particle energy) this nonlinear equation can be solved for the equilibrium temperature of the heated atmosphere. Note that the expression is quadratic in N_{21}, so that finding N_{21} as a function of F_{b} and T is relatively simple. In Fig. 7 we show the equilibrium temperature as a function of F_{b} and N. For a large range of parameter values the temperature varies between 7000 K and approximately 18000 K. These values are in the correct range to explain optical flares. The insensitivity of the temperature to the values of F_{b} and N is caused by the ionization which acts as a thermostat. Only for small values of N and high values of F_{b} (upper left corner of the figure) are much higher temperatures found. In that case only a relatively small fraction of the beam energy goes into ionization losses and the bulk of the beam energy goes into heating.

The black-body temperature of the optical flare (T_{bb}) is related to the flare magnitude ($\triangle m$) in the U-band according to

$$10^{\triangle m/2.5} = \frac{A_{\text{f}} B(T_{\text{bb}}) + (A_* - A_{\text{f}}) B(T_*)}{A_* B(T_*)}$$
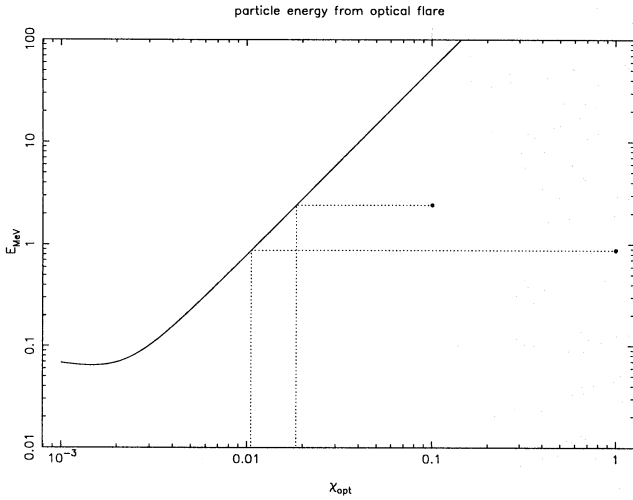
particle energy from optical flare

Fig. 8. Particle energy as a function of dimensionless optical flare area χ_{opt} (solid line). Also indicated are the particle energies as derived from the radio data (dots).

$$= \chi_{opt} \frac{B(T_{bb})}{B(T_*)} + 1 - \chi_{opt} \qquad (11)$$

with A_* the stellar disk area, A_f the optical flare area, $B(T)$ the Planck function, $T_* = 3250$ K the effective temperature of the star, and $\chi_{opt} = A_f/A_*$.

Eq. (11) indicates that the black-body temperature of the flare is a simple function of the dimensionless optical flare area χ_{opt}. In the two-ribbon flare scenario the optical emission occurs during the impulsive phase of the flare when the current sheet is at a relatively low altitude. The particles responsible for the optical flare hit the atmosphere over an area $A_f = \chi_{opt}A_*$ and carry all the energy for the optical emission so that

$$A_f F_b t_{inj} = E_{opt} , \qquad (12)$$

where t_{inj} is the duration of the beam bombardment, E_{opt} is the total flare energy at optical wavelengths and $F_b = n_f \beta c E$ is the beam flux with n_f the beam particle density. Taking $t_{inj} \approx 110$ s, equal to the duration of the rise phase of the optical flare, and $E_{opt} \approx 2\ 10^{32}$ erg, the total energy losses in the U-band, the beam flux becomes a simple function of the optical flare area

$$F_b = 4\ 10^8 \chi_{opt}^{-1} . \qquad (13)$$

Consider χ_{opt} now as a variable. For a given value of χ_{opt} we obtain from Eq. (13) the beam flux and from Eq. (11) the black-body temperature of the flare. Inserting this temperature and the value for the beam flux into Eq. (10) gives the required column density N_{21}, which is related to the beam particle energy E by Eq. (7). The result is presented in Fig. 8, where the solid line indicates the particle energy as a function of χ_{opt}. All the combinations of E and χ_{opt} on this line result in a correct value for the U-band losses. The range of values that E can take, however, is limited by the radio data. In Fig. 8 the dots indicate the implied particle energies for two typical, but assumed, sizes of the

Table 5. Results for two values of the assumed radio source size (χ_r).

χ_r	0.1	1
E (MeV)	$2.4/\sqrt{B_2 \sin\vartheta}$	$0.9/\sqrt{B_2 \sin\vartheta}$
N_{21}	750	97
χ_{opt}	$1.85\ 10^{-2}$	$1.05\ 10^{-2}$
T_{bb} (K)	8427	9561
F_b (erg/s/cm^2)	$2.2\ 10^{10}$	$3.9\ 10^{10}$
n_f (cm^{-3})	$1.9\ 10^5$	$9.2\ 10^5$

radio source at the maximum of the 6 cm flux. With the assumption that both the optical flare and the radio flare are caused by particle populations with comparable energies we find that the optical flare area varies between $\chi_{opt} \approx 1.9\ 10^{-2}$ for $\chi_r = 0.1$ and $\chi_{opt} \approx 10^{-2}$ for $\chi_r = 1$. The corresponding black-body temperature varies between approximately 8427 K and 9561 K (see Table 5). These values compare favourably with previous (spectroscopic) observations of flares on YZ CMi. Mochnacki and Zirin (1980) found for a flare that $\chi_{opt} \lesssim 10^{-2}$ with the flare continuum well fitted with a dominant black-body component and with a smaller contribution by a hydrogen recombination component. Kahler et al. (1982) found that at the maximum of an optical flare the emission could well be fitted with a black-body spectrum with $T_{bb} = 8500$ K and $\chi_{opt} = 5\ 10^{-3}$. Although for the present observation only the U-band flux is available, more detailed observations sometimes indicate the presence of black-body emission that supports this interpretation. It is likely, however, that a black-body signature only arises when the beam particles deposit their energy deep enough in the atmosphere while the beam flux is still large. In the present case the MeV electrons deposit their energy (up to) close to the temperature minimum in the atmospheric model for YZ CMi by Giampapa et al. (1982). The results presented in Fig. 8 show that both the particle energy and the optical flare area are not extremely sensitive to the assumed size of the radio source. Because the beam flux and the energy of the beam particles are known, it is possible to calculate the density of the energetic particles assuming they move with a velocity $\beta = 1$. The derived density is in the range $n_f \approx 2-9\ 10^5$ cm^{-3} (see Table 5). In Sect. 3.2 we found that if the source is optically thick, $n_f \ell \gtrsim 2\ 10^3$ cm^{-2}. With the given values of n_f we find that ℓ must larger that 0.01, a condition which is easily met.

The typical size of the optical flare area ($\sim 0.01 A_* = 2\ 10^{19}$ cm^2) is a factor 33 larger than the area of solar white light flares at flare maximum ($\sim 6\ 10^{17}$ cm^2, Neidig and Cliver, 1983). Machado and Rust (1974) observed a solar white light continuum with temperatures in the range 8,500 - 20,000 K, comparable with the temperature range indicated in Fig. 7. The white light power amounted to a few times 10^{27} erg s^{-1} during the impulsive phase. In our case the U-band peak luminosity amounts to 10^{30} erg s^{-1}. Because the solar white light flare and the present flare have comparable temperatures, the larger luminosity in the U-band can only be explained if the stellar optical

flare area is considerably larger than the typical value for solar white light flares, as indeed is found.

The above derived optical flare area of $\sim 2\ 10^{19}$ cm^2 may be compared with that based on the UV observations. For example, taking the radiative power output in the UV lines of C IV 1550Å, Si IV 1396Å, C III 1176Å, and the line emissivities of Doyle and Keenan (1992), we derive a mean (volume) emission measure of $2.5 \pm 0.1\ 10^{49}$ cm^{-3} for the flare plasma. Assuming a simple cube structure, this translates to a flare area of $\sim 1.6\ 10^{19}$ cm^2 (based on the derived electron density from the C III lines in Sect. 3.3), which is in good agreement with the above derived optical flare area.

Although the results present in Table 5 show that a combined interpretation of the optical and the radio data results in reasonable parameters, especially when compared with other flare observations, some critical remarks are appropriate. The first point we would like to address is the use of the U-band. The flux in this band contains a substantial contribution by higher members of the Balmer series, the Balmer continuum, the Balmer jump and Ca II H & K (see discussion by Giampapa, 1983, and Worden, 1983). Although it may contain a black-body component, the true spectrum is unlikely to consist only of black-body radiation. The optical flare area $\chi_{\rm opt}$, as determined from Eq. (11) must therefore be considered as an *effective* area for black-body radiation similar to the procedure followed by Mochnacki and Zirin (1980) and Kahler et al. (1982).

Unfortunately, since there were no X-ray observations for this event it is difficult to say anything concerning the thermal electrons in the corona. It has been suggested by various authors (based on the results of Hartmann et al., 1979, 1982) that the UV line of He II 1640Å can be used to obtain information about the X-ray plasma since the Hartmann et al. produced calculations to show that, with increasing magnetic activity, the He II 1640Å line is dominated by recombination. However, an analysis by Seely and Feldman (1985) of solar quiet and active regions and of flaring plasma showed that this is not the case. This conclusion is at variance with the recent radiative transfer calculations of Wahlstrom and Carlsson (1994) who showed that this line is formed by photoionization from the ground state of He II, mainly by the incident of EUVE radiation. Assuming that 60% of the He II 1640Å emission is due to recombination (Hartmann et al. 1982), and using the relation between the X-ray flux and the He line flux (Hartmann et al. 1979), suggests an X-ray flux of $\sim 8\ 10^{-12}$ erg cm^{-2}s^{-1} during the 40 min. IUE exposure and a total X-ray radiative losses of $\sim 10^{32}$ erg. This flux should be considered as a lower limit as it only refers to the narrow spectral range as covered by the Einstein IPC. A study by Pallavicini et al. (1990) using the EXOSAT LE detector, indicates total X-ray energies in the range $0.66 - 2.8\ 10^{32}$ erg for three flares on YZ CMi. Although in principle the thermal X-ray flare radiative losses can be comparable to the optical losses we do not elaborate on this further given the uncertainties in the formation of the He II 1640Å line.

The deceleration of the energetic electrons in the atmosphere results in the emission of non-thermal thick target X-ray emission (Brown, 1971). The ratio of the total radiative losses during
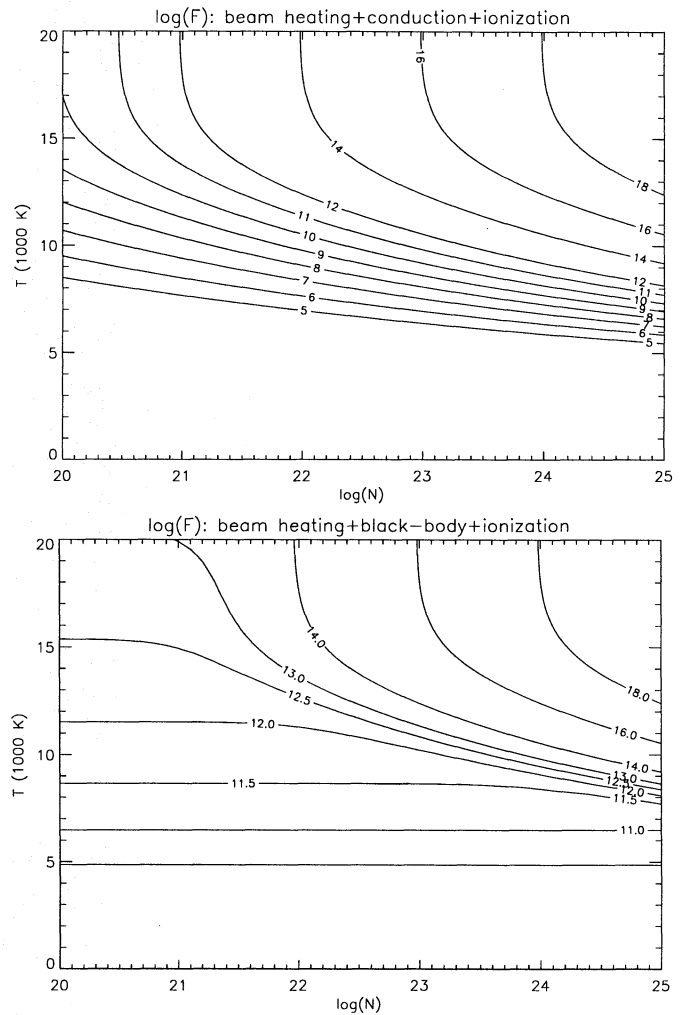

Fig. 9. Beam flux as a function of column density N and equilibrium temperature T. The results in the top panel are based on a balance between beam heating and conductive and ionization losses. The results in the lower panel follow from the balance between beam heating and black-body and ionization losses. Note the substantial higher beam fluxes which are required to obtain a given equilibrium temperature when black-body losses are important.

the braking process $E_{\rm rad}$ and the (initial) kinetic power is the beam $E_{\rm beam}$ is in the thick target approximation given by

$$\frac{E_{\rm rad}}{E_{\rm beam}} = \frac{4}{3}\frac{\alpha}{\pi}\frac{E}{mc^2}\frac{1}{\Lambda} \approx 1.5\ 10^{-4}\left(\frac{\Lambda}{20}\right)^{-1}\frac{E}{mc^2}$$

where α is the fine structure constant and E is the electron's energy at the moment of injection. This expression shows that MeV electrons loose a negligible fraction of their energy in the form of X-ray Bremsstrahlung and that practically all energy is lost by collisions resulting in heating of the ambient medium.

Our model predicts the creation of a heated plasma column in the lower chromosphere/photosphere. The column depth over which the heating occurs lies in the range $23 \lesssim \log N \lesssim 24$, which is determined by the typical particle energy required by the observed radio flux. The other input parameter is the beam

flux (Eq. (13)) in which there are two sources of uncertainty: the total optical energy losses, for which the energy must be supplied by the beam, and the flare area. Because the flare area is only an effective area, derived under the assumption of black-body emission, it may differ from the actual flare area. The total energy losses are probably larger than the value we used because we used the total losses in only the U-band. The resulting uncertainty in the beam flux will, however, not considerably change our results. To demonstrate this we present in Fig. 9a the beam flux as a function of column density and equilibrium temperature. This figure is another presentation of the data in Fig. 7. The figure clearly shows that in the range $23 \lesssim \log N \lesssim 24$ the equilibrium temperature is relatively insensitive to the assumed beam flux. We calculated, for example, the parameters given in Table 5 using a ten times higher value for E_{opt}. The resulting temperatures were only 500 - 800 K higher than those listed in Table 5, while the optical flare area was only 25% smaller. Our results are, therefore, not very sensitive to our underestimate of the beam flux.

An indication of how the actual optical spectrum may look can be obtained from the results of Donati-Falchi et al. (1985), who calculated the optical spectrum of solar flares in the wavelength range 3600-4000Å. The temperature range considered in their calculations was $7 - 12 \ 10^3$ K, the electron density range $13.1 \leq \log n_e \leq 13.5$, and the hydrogen slab depth 400 and 500 km. These values are considered to be typical for solar flares. How does this compare with our parameters? The column densities we found correspond to geometrical sizes in the range 420-450 km in the model chromosphere for YZ CMi (see Giampapa et al., 1982). The electron density can be estimated using $n_e = (f/(f+1))N_H \approx 2 \ 10^{-7}(f/(f+1))N$ (see discussion below Eq. (9)). For $T = 8427$ K we find $n_e = 1.9 \ 10^{13}$ cm^{-3} and for $T = 9561$ K we find $n_e = 2.6 \ 10^{13}$ cm^{-3}. Despite the simplicity of our model, these parameters fit surprisingly well within the range of typical solar flares parameters. The models by Donati-Falchi et al. can, therefore, be used to obtain an impression of how the actual spectrum looks. We refer to Figs. (1) and (3) by Donati-Falchi et al. which show part of the spectrum in the U-band range. The presence of higher members of the Balmer series dominate these spectra with the highest members merging into a pseuso-continuum.

The applicability of Eq. (9) is limited by its inclusion of only bound-free transitions. Because of the assumed equilibrium between collisional ionization and radiative recombinations these kind of transitions are automatically included. At the calculated equilibrium temperatures the number of recombinations amounts to $3.8 \ 10^{40}$ s^{-1} for the whole optical flare volume. The losses in the Balmer lines are not included but will probably not strongly change the results. This can be seen as follows. The inclusion of bound-bound radiative losses will on average correspond to a correction factor in Eq. (9) in the term for the ionization losses. But this corresponds to using Eq. (9) with a lower beam flux. Above we demonstrated that the resulting equilibrium temperature is insensitive to changes of the beam flux by say a factor ten. Therefore the inclusion of bound-bound transitions will not significantly change our results.

We would like to add a few remarks concerning the application of black-body radiation in stellar flare models. Assume first that the flaring region actually emits a black-body spectrum. In that case we should include an extra term $-\sigma T^4$ in Eq. (9) with σ the Stefan-Boltzmann constant. Such a term makes the conductive losses unimportant for the global energy balance. In Fig. 9b we present the beam flux as a function of the column density and the equilibrium temperature with the beam fluxes now calculated using Eq. (9) with the conductive losses replaced by black-body losses. There is a striking difference with the results presented in Fig. 9a. To achieve equilibrium temperatures for the flaring volume near 10,000 K, a much higher beam flux is required. In an equilibrium situation the beam flux must at least be larger than or equal to the black-body emittance: $F_b \gtrsim \sigma T^4 = 5.7 \ 10^{11}T_4^4$ erg cm^{-2}s^{-1} or $T \lesssim 6480F_{b,11}^{1/4}$ K. This shows that only very energetic beams can produce black-body temperatures of ~ 8500 K as was oberved by Kahler et al. (1982). In other words, the model we used will more easily explain an optical flare than a model with black-body losses. For dMe-stars, which show frequent optical flare activity, it is therefore likely that the radiative losses are not similar to a black-body because each of the observed flares would require very energetic electron beams. We note that for a black-body spectrum at most 10% of the black-body emittance is detected in the U-band. This occurs for 8000 K $< T_{bb} <$ 12000 K. At other temperatures this fraction is much less. This implies that if a black-body spectrum is observed in the U-band, a large fraction of the radiative losses are outside of the band.

The radio flux peaks about 7 minutes after the optical maximum. During this time interval the flaring structure expands from an area given by χ_{opt} to χ_r. The linear expansion velocity (proportional to $\sqrt{\chi}$) corresponds to $v = 110$ km s^{-1} for χ : $1.85 \ 10^{-2} \rightarrow 0.1$ and $v = 550$ km s^{-1} for χ : $1.05 \ 10^{-2} \rightarrow 1$. From the decay of the radio flare we estimated the coronal density to be $n \approx 10^9$ cm^{-3} so that the Alfvén velocity corresponds to $v_A = 6900B_2/\sqrt{n_9}$ km s^{-1}. These expansion velocities correspond to $0.016v_A$ and $0.08v_A$. These numbers indicate that typical velocities of a few hundred kilometer per second are involved, which are also typical for erupting solar filaments. The velocity that the erupting filament can obtain is set by the rate at which magnetic field lines are transported into the current sheet, since this is the rate at which the field lines which hold the filament down are reconnected. Models for magnetic reconnection predict inflow velocities in the range of 1-10% of the Alfvén velocity (Petschek, 1964) consistent with our estimates.

The sub-Alfvénic velocities imply that the filament evolves almost force-free. This does not come as a surprise, because the Lorentz force on a filament is so large that enormous accelerations would occur if the filament were not close to the force-free state. Another way of putting this is that the filament constitutes a (O-type) neutral point in the magnetic configuration which by definition must be (almost) force-free.

The pre-flare evolution of a filament is governed by the balance of two strong but opposite Lorentz forces (van Tend and Kuperus, 1978): a downward force by the (background) active

region magnetic field on the filament current, and the upward force by an induced surface current distribution. The origin of this surface current results from the inability of the (frozen-in) coronal magnetic field to re-enter the photosphere which has a much larger intertia than the plasma in the coronal magnetic field. The photosphere, therefore, acts as a boundary (separatrix) between topologically different flux systems along which currents are induced. The effects on the coronal magnetic field by these surface currents can be modeled by placing a virtual current below the photosphere which is equal and opposite to the filament current (Kuperus and Raadu, 1974). The force balance on the filament is then

$$\frac{I}{c}\left(\frac{I}{cz} - B(z)\right) = 0$$

with I the filament current, z the height of the filament and $B(z)$ the active region magnetic field. At heights where $B(z)$ drops faster than $1/z$, no stable equilibrium is possible and a flare occurs (see van Tend and Kuperus, 1978). The point of instability is also close to the moment that a neutral line emerges above the photosphere whose presence allows the magnetic reconnection process to start.

At the moment that the instability occurs we have from the above equation $I = czB$, where all quantities relate now to the critical values at the moment of instability onset. Let h_s now define the height of the current sheet, h_f the height of the filament, and ℓ the length of the filament. Numerical simulations (Kaastra, 1985, Martens and Kuin, 1989) indicate that $h_s \approx 0.1h_f$. We write $\ell = \rho h_f$ with $\rho \approx 4 - 6$ for solar filaments. In the following we apply these relationships, based on models for solar two-ribbon flares, to obtain information on the reconnection process during the flare on YZ CMi. We take for the length over height ratio a canonical value $\rho = 5$ indicated by ρ_5 and for the dimensionless optical flare area a value $\chi_{opt} = 10^{-2}$ indicated by χ_{-2}.

Below the current sheet a semi-cylindrical arcade of loops is formed during the flare with a radius h_s. The optical flare area corresponds then to approximately $\chi_{opt}A_* = 2h_s\ell$ from which we find $h_f = 45.6\sqrt{\chi_{-2}/\rho_5}$ Mm and $\ell = 228\sqrt{\rho_5\chi_{-2}}$ Mm. The total energy in the system is given by $W = LI^2/2$ with $L \approx \ell/c^2$ the self-inductance. Taking $I = ch_fB$, we obtain $W = 2.4 \ 10^{33}B_2^2\chi_{-2}^{3/2}\rho_5^{-1/2}$ erg. This energy is comparable to the total radiative losses during the flare, but it must be considered as a lower limit because, as the reconnection proceeds, an area larger than χ_{opt} can become involved. It demonstrates, however, that enough energy is available to power the impulsive phase of the flare.

We found that the typical velocity with which the system expands is about one hundred kilometers per second. We denote this expansion velocity as v_7. The expansion results in a change of the self-inductance of the system and as a consequence an inductive voltage V is present in the current sheet. This voltage is given by

$$V = I\frac{dL}{dt} = \frac{I}{c^2}\frac{d\ell}{dt} \approx \frac{I}{c}\frac{v}{c} = h_fB\frac{v}{c}$$

$$= 1.5 \ 10^8 B_2 v_7 \chi_{-2}^{1/2}\rho_5^{-1/2} \text{ statvolt} \tag{14}$$

and the related electric field amounts to $E = V/\ell = 6.7 \ 10^{-3}B_2v_7/\rho_5$ statvolt cm^{-1}. This value is comparable to the value of $1.5 \ 10^{-2}$ found in the numerical model by Martens and Kuin (1989) and to the observationally derived value of $8.3 \ 10^{-3}$ by Kopp and Poletto (1986).

The fraction of particles which experiences run-away aceleration in the current sheet can be estimated by comparing the electric field with the Dreicer field E_D. In the current sheet the resistance will become anomalous and for the effective collision frequency we take the canonical value $\nu \approx 0.01\omega_p$ (Vlahos and Papadopoulos, 1979) with $\omega_p = 2\pi\nu_p$. Earlier we found that $\nu_p \approx 0.3$ GHz. The Dreicer field now follows from

$$E_D = \frac{4\pi\nu}{\omega_p^2}nev_t = 12.5 \ 10^{-3}\left(\frac{T_6}{n_9}\right)^{1/2} \text{ statvolt cm}^{-1}, \tag{15}$$

with v_t the electron thermal velocity, so that $E/E_D \approx 0.54$. For a given value of the ratio E/E_D, the fraction of runaway particles is estimated by Norman and Smith (1978) to be

$$\frac{N_r}{N} = \frac{1}{2}\exp\left(-\frac{1}{2}\left[\left(\frac{E_D}{E}\right)^{1/2} - \frac{E}{E_D}\right]^2\right). \tag{16}$$

For $E/E_D \approx 0.54$ this expression gives $N_r/N \approx 0.36$, implying that about one third of the electrons entering the sheet are accelerated. Is this value consistent with our previous results? The total number of electrons entering the sheet per second is approximately given by

$$2h_s\ell nv = 2.1 \ 10^{35}n_9v_7 \text{ electrons s}^{-1},$$

while the total number of accelerated electrons per second can be estimated from

$$\chi_{opt}A_*n_fc = 1.2 \ 10^{35}\left(\frac{n_f}{2 \ 10^5}\right) \text{ electrons s}^{-1}.$$

These numbers imply that $N_r/N \approx 0.57$ which is surprisingly close, given the uncertainties, to the value of 0.36 which followed from the independent estimate of the electric field.

We conclude that the observed flare on YZ CMi shows a strong similarity with the two-ribbon flares observed on the Sun.

5. Conclusions

In this paper we have discussed combined observations of YZ CMi at optical, UV and radio wavelengths. YZ CMi was found to undergo repeated optical flaring. The most outstanding result is the 3.8 magnitude flare which occured on 3 February 1983. This flare coincided exactly with an IUE exposure and showed a clear radio counterpart. As a result we were able to construct emission measure curves for the temperature range $4.0 \leq \log T_e \leq 5.4$ during the flare and to compare these with similar curves for YZ CMi in its quiescent state (Fig. 5). At those locations in the atmosphere were strong temperature gradients are present, like e.g. the transition region, the emission

measure will have a relatively low value. In Fig. 5 it is clear that during the flare the position of the transition zone has shifted from $T = 10^5$ K in quiescence to $T \approx 10^{4.8}$ K and that the overall height of the emission measure curves increased. This behaviour is consistent with the scenario in which the flare energy release takes place in the corona. By means of particle beams or a conductive flux, part of the flare energy is transfered to the chromosphere which heats up, implying a downward shift of the transition region. This downward shift, associated with chromospheric evaporation, implies that at each temperature the density effectively increases so that the radiative losses at each temperature increase (Fig. 6).

During the flare the radio flux at 6 cm peaks about seven minutes after the U-band flux. The absence of radio emission at 20 cm can be understood if the radio emission mechanism is optically thick synchrotron emission by MeV electrons in coronal fields of about 100 Gauss. In order to explain the absence of emission at 20 cm, there is no need to invoke a coherent emission mechanism or flux reduction by means of Razin suppresion. The collisional time scale (Eq. (6)) indicates that the MeV electrons move in a medium with a typical coronal density of $n \approx 10^9$ cm^{-3}.

The lack of spatial resolution makes it difficult to compare stellar flares with the better observed solar flares. One can at most make a comparison between the global characteristics. In this paper we used the global characteristics of the solar two-ribbon/white-light flare to model the combined optical/radio flare. Our basic assumption is that the reconnection process results in an energetic particle distribution with a typical energy determined by the reconnection process. These energized particles are then responsible for both the radio and the optical flare. From the interpretation of the radio flare we found that this typical particle energy is a few MeV for typical values of the source size. The particles trapped in the corona loose their energy by collisions and give rise to the synchrotron emission at 6 cm.

The MeV electrons which precipitate in the loss cone can cross a substantial column depth before they are stopped. During the braking process their energy is transferred to the ambient medium which is then ionized and heated. In order to calculate the physical parameters of the bombarded atmospheric column, we applied the relatively simple model proposed by van den Oord (1988) which considers only the global energy balance of the atmospheric column and does not include any dynamics. In the bombarded column an equilibrium is established, on a short time scale, between beam heating, ionization losses and conductive losses. Although the model is rather crude, it has some very interesting implications. First of all, the equilibrium temperature reached in the plasma column is mainly determined by the energy of the beam particles, and therefore the stopping depth N, while this temperature is fairly insensitive to the actual beam flux (see Figs. 7 and 9). Secondly, the equilibrium temperatures are in the range (7.000 - 20.000 K) found for solar white-light flares. The insensitivity of the equilibrium temperature to the actual value of the beam flux implies that during both weak and strong flares on YZ CMi, the same atmospheric

conditions are created which favour emission at optical wavelengths. The difference between weak and strong flares can then be related to the typical energy of the particles and hence to the column depth involved.

To derive the characterictics of the optical flare we assumed that the emission is black-body. With this assumption an *effective* optical flare area is found which is comparable with the earlier results for YZ CMi by Mochnacki and Zirin (1980) and Kahler et al. (1982). The results of the combined optical/radio interpretation, given in Table 5, must be regarded as typical parameters. Even though the radio source size is unknown, the Table shows that there is a surprisingly small spread in the derived parameters. This is caused by the insensitivity of the equilibrium temperature to the magnitude of the beam flux. The reason for this behaviour is that in cool dwarf atmospheres the balance between ionization and radiative recombination acts as a very efficient thermostat. Only when the beam energy is deposited at very small column depths, where the plasma is already ionized, does this mechanism not work and strong temperature increases result.

We demonstrated that it unlikely that the actual radiative losses are truely black-body and we only used an equivalent black-body radiator to derive an effective flare area. If the radiative losses would in reality be black-body, then high beam fluxes are required to heat the bombarded plasma column to typical white-light flare temperatures (Fig. 9, lower panel). The reason is that a black-body is a very efficient emitter ($\sim T^4$), so that a large energy deposition is required to increase the temperature. With the frequent optical flaring of YZ CMi it is unlikely that each of these flares would be characterized by the presence of beams with $F_b \gtrsim 10^{11}$ erg cm^{-2}s^{-1} although detailed spectroscopic observations of flares during their impulsive phase are required to see whether black-body emission can in reality be ruled out.

The results listed in Table 5 indicate that the derived parameters fit nicely within the parameter range considered by Donati-Falchi et al. (1985) for solar white-light flare modeling. Their model predicts a strong increase of the Balmer lines which actually has been observed on YZ CMi during a flare (Doyle et al. 1988, see their Figs. 2 and 10). In order to arrive at a quantitative comparison, however, better spectroscopic observations are required. This point has been extensively discussed by Houdebine (1992) who also addresses the role of MeV electrons in stellar flares. We note however that Houdebine made no allowance for changes in the ionization fraction during the beam bombardment while in our model the ionization acts as a thermostat in the bombarded plasma column.

In addition to comparing the observed flare with the solar white-light flare, we also checked whether the observed flare can be interpreted consistently as a two-ribbon flare. The increase of the radio flux is then interpreted as due to a growing arcade of loops, forming below a current sheet, which emit synchrotron radiation. The typical velocity is of the order of a few hundred kilometers per second as has been observed for erupting solar filaments. In the current sheet the value of the electric field is comparable to the values derived, both theoretically and obser-

vationally, for solar two-ribbon flares. Moreover, the predicted number of electrons which experience run-away acceleration in the current sheet is of the same order as is required to power the optical flare.

We conclude that the observed optical and radio flare can be interpreted within the (global) framework of solar two-ribbon flares with the optical flare volume showing strong resemblances with the atmospheric conditions created during solar white-light flares.

References

Benz, A.O., Gold, T., 1971, Solar Phys. 21, 157

Bessell, M.S., 1979, PASP, 91, 589

Brown, J.C., 1971, Solar Phys., 18, 489

Bruner, M.E., McWhirter, R.W.P., 1988, ApJ, 326, 1002

Butler, C.J., Rodonò, M., Foing, B.H. & Haisch, B.M., 1986, Nat, 321, 679

Butler, C.J., Doyle, J.G., Andrews, A.D. et al., 1987, A&A, 174,139

Cook, J.W., Cheng, C.C., Jacobs, V.L. & Antiochos, S.K., 1989, ApJ 338,1176

De Jager, C., et al., 1988, A&A 156,95

Donati-Falchi, A., Falciani, R., Smaldone, L.A., 1985, A&A, 152, 165

Doyle, J.G., Butler, C.J., Byrne, P.B. & van den Oord, G.H.J., 1988, A&A, 193,229

Doyle, J.G. 1989, A&A, 214,258

Doyle, J.G., Byrne, P.B. & van den Oord, G.H.J., 1989, A&A, 224,153

Doyle, J.G. & Keenan, F.P., 1992, A&A, 264,173

Emslie, A.G., 1978, ApJ, 224, 241

Forbes, T.G., 1990, J. Geoph. Res., 95, 11919

Forbes, T.G., 1991, Geoph. Astroph. Fluid Dynamics, 62, 15

Forbes, T.G., Isenberg, P.A., 1991, ApJ, 373, 294

Gershberg, R.E., 1972, Ap&SS, 19, 75

Giampapa, M.S., Worden, S.P., Linsky, J.L., 1982, ApJ, 258, 740

Giampapa, M.S., 1983, in: Activity in red-dwarf stars, eds. P.B. Byrne, M. Rodonò, Reidel, Dordrecht, p. 223

Giddings, J. & Rees, P., 1989, SERC Starlink User Note, No. 37

Gliese, W., 1969, *Catalogue of Nearby Stars*, Veroff der Astron Rechen-Inst, Heidelberg, No. 22

Haisch, B.M., Rodonò, M., (eds.), 1989, *Solar and Stellar Flares*, Proc. IAU Coll. 104, Sol. Phys., 121

Haisch. B.M., Strong, K.T., Rodonò, M., 1991, ARA&A, 29, 275

Haisch, B.M., Linsky, J.L., Bornmann, P.L., Stencel, R.E., Antiochos, S.K., Golub, L. & Vaiana, G.S., 1983, ApJ, 267, 280

Haisch, B.M., Butler ,C.J., Doyle, J.G. & Rodonò, M., 1987, A&A, 181, 96

Hartmann, L., et al., 1979, ApJ, 233, L69

Hartmann, L., Dupree, A.K. & Raymond, J.C., 1982, ApJ, 252, 214

Houdebine, E.R., 1992, Irish Astron. J., 20, 213

Houdebine, E.R., Foing, B.H., Doyle, J.G. & Rodonò, M., 1993a, A&A, 274, 245

Houdebine, E.R., Foing, B.H., Doyle, J.G. & Rodonò, M., 1993b, A&A, 274, 245

Howarth, I.D. & Murray, J., 1990, Starlink Users Note No. 50

Kaastra, J.S., 1985, Solar Flares: an electrodynamical model, Thesis Utrecht University

Kahler, S., et al., 1982, ApJ, 252, 239

Kopp, R.A., Poletto, G., 1986, in: Coronal and prominence plasmas, ed. A. Poland, NASA CP-2442, p. 469

Kunkel, W.E., ApJ, 161, 503

Kuperus, M., Raadu, M.A., 1974, A&A, 31, 189

Lacy, C.H., Moffett, T.J., Evans, D.S., 1976, ApJS, 30, 85

Linsky, J.L., Neff, J.E., Brown, A., Gross, B.D., Simon, T., Andrews, A.D., Rodonò, M. & Feldman, P.A., 1989, A&A, 211, 173

Linsky, J.L., et al., 1995, ApJ, 442, 381

Machado, M.E., Rust, D.M., Solar Phys., 38, 499

Maran, S.P., et al., 1994, ApJ, 421, 800

Martens, P.C.H., 1986, Solar Phys., 107, 95

Martens, P.C.H., Kuin, N.P.M., 1989, Solar Phys., 122, 263

Mathioudakis, M., Doyle, J.G., 1992, A&A, 262, 523

Meyer, J.P., 1985, ApJS, 57, 173

Mochnacki, S.W., Zirin, H., 1980, ApJ, 239, L27

Neidig, D.F., Cliver, E.W., 1983, AFGL-TR-83-0257, Hanscom AFB, MA.

Norman, C.A., Smith, R.A., 1978, A&A, 68, 145

Pacholczyk, A.G., Radio Astrophysics, W.H. Freeman and Company

Pallavicini, R., Tagliaferri, G., Stella, L., 1990, A&A, 228, 403

Petschek, H.E., 1964, in: Symposium on the physics of solar flares, NASA-SP 50, ed W.N. Hess, p. 425

Pettersen, B.R., (ed.), 1991, *Stellar Flares* in Mem Soc Astr Ital 62, no.2

Quin, D.A., Doyle, J.G., Butler, C.J., Byrne, P.B. & Swank, J.H., 1993, A&A, 272, 477

Rodonò, M., et al., 1984, 4th Eur. IUE Conf., ESA SP-218, 247

Rodonò, M., et al., 1989, Proc. IAU Coll. 104 on *Solar and Stellar Flares*, Poster Papers, Catania Ap. Obs. Special Publ., p. 53

Seely, J.F.,Feldman, U., 1985, MNRAS 213, 417

Syrovatskii, S.I., 1981, ARA&A, 19,163

Tucker, W.H., 1975, Radiation processes in Astrophysics, MIT Press, Cambridge, Massachusetts, p. 290

van den Oord, G.H.J., 1988, A&A, 207, 111

van den Oord, G.H.J., de Bruyn, A.G., 1994, A&A, 286, 181

van Tend, W., Kuperus, M., 1978, Solar Phys., 59, 115

Vlahos, L., Papadopoulos, K., 1979, ApJ, 233, 717

Wahlstrom, C., Carlsson, M., 1994, ApJ, 433, 417

Wolfson,C.J., Doyle, J.G., Leibacher, J.W., Phillips, K.H.J., 1983, ApJ, 269, 319

Worden, S.P., 1983, in: Activity in red-dwarf stars, eds. P.B. Byrne, M. Rodonò, Reidel, Dordrecht, p. 207